PERGAMON

Journal of Structural Geology 25 (2003) 241–252

JOURNAL OF STRUCTURAL GEOLOGY

www.elsevier.com/locate/jsg

Are the solutions of stress inversion correct? Visualization of their reliability and the separation of stresses from heterogeneous fault-slip data

A. Yamaji*

Division of Earth and Planetary Sciences, Graduate School of Science, Kyoto University, Sakyo-ku, Kyoto 606-8502, Japan

Received 28 March 2001; revised 20 January 2002; accepted 30 January 2002

Abstract

It is now a conventional technique to determine the optimal stress from fault-slip data by inversion. However, the method is weak when applied to heterogeneous data. A new technique is presented here to visualize the reliability of the solution. It is also shown that the technique allows us to separate stresses from those data. The technique is simple: it is the visualization of the object function of the inversion. The present method is compared with the conventional inverse method and the multi-inverse method using artificial and natural heterogeneous data sets. The conventional method can determine one of the stresses, if the orientation of the faults has a large variation. It is shown that the solutions of the method are non-unique and unstable for some data sets, indicating that they are not reliable. The present graphical method and multi-inverse method are more robust than the conventional one for heterogeneity. The multi-inverse method seems to have better resolution than the present method. However, unlike the multi-inverse method, the time of computation of the present method does not increase with the number of faults, so that the method becomes favorable for processing hundreds of faults. © 2002 Elsevier Science Ltd. All rights reserved.

Keywords: Stress inversion; Fault slip data; Polyphase tectonics; Tectonic stress

1. Introduction

The estimation of tectonic stress is important for structural geologists to contribute to geodynamic studies (Pollard, 2000), to foundation engineering (Amadei and Stephansson, 1997), and to estimate subsurface fluid flow (Nelson, 1985; Mandl, 2000). Since Carey and Brunier (1974) and Angelier (1979), fault-striation analysis has been a conventional tool for this purpose in sedimentary basins and in fractured crystalline basement over the world. Most of the inversion methods are based on the Wallace–Bott hypothesis that slip vectors are parallel to the resolved shear stress on the faults (Wallace, 1951; Bott, 1959), and determines the optimal stress by an inverse method from fault-slip data obtained from outcrops, from shear factures in bore-hole cores (Dezayes et al., 1995; Martin and Bergerat, 1996), or from seismic focal mechanism data (McKenzie, 1969; Angelier, 1984; Gephart and Forsyth, 1984).

However, there are serious drawbacks in this method that are sometimes overlooked. The Wallace–Bott hypothesis fails in interacting and closely spaced faults (Dupin et al., 1993; Pollard et al., 1993; Nieto-Samaniego and Alaniz-Alvarez, 1997) and in faults with significant block rotations (Twiss and Unruh, 1998). A macroscopic rock mass undergoes irreversible deformation by the activity of mesoscale faults in the mass. Faulting itself results in discontinuous movement across the fault plane; however, we have to disregard the effects of individual faults and resort to a macroscopic plasticity theory to describe the deformation of the mass. Materials with such a macroscopic behavior are called frictional plastic solids (Mandl, 2000). Palesotresses are correctly determined from mesoscale faults if the rock mass has linear and isotropic plasticity in macroscopic view (Twiss and Unruh, 1998).

Given the Wallace–Bott hypothesis to be correct, are the solutions of the inverse method reliable? The popular and classic inverse method typified by those of Angelier (1979, 1984, 1990) and Gephart and Forsyth (1984) determines only one stress from a given fault assemblage. The optimal solution is determined as the maximum point of a function in four-dimensional parameter space (Angelier, 1990). Such a function is called the object function in inverse theory. The reliability depends on the stability and uniqueness of the solution. The solution is called unstable if the optimal stress is altered completely by the subtraction of a small number of fault-slip data from the given data set or by the addition of a

* Tel.: +81-75-753-4150; fax: +81-75-753-4189.
E-mail address: yamaji@kueps.kyoto-u.ac.jp (A. Yamaji).

0191-8141/02/$ - see front matter © 2002 Elsevier Science Ltd. All rights reserved.
PII: S0191-8141(02)00021-4

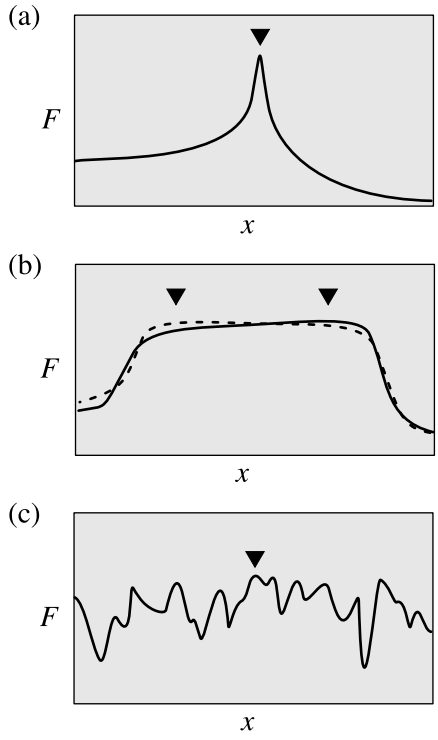

Fig. 1. Schematic pictures showing the stability and uniqueness of the optimal point. Inverse methods seek the optimal (maximum) point of the object function, $F(x)$. The pictures show the graph of the function. The maximum point (triangle) represents the optimal solution of inversion. (a) Uni-modal, convex function with a narrow peak. In this case, the solution is stable and unique. (b) Function with a plateau. A small variation in the topography (smooth and dotted lines) results in shift of the peak at a long distance. The optimal solution indicated by the peak is unstable. (c) Multi-modal function. In this case, the solution is not unique. In addition, the peaks have similar height, resulting in an unstable optimal solution. Reliability of the solution is not warranted by the fact that it is the highest.

small number of them to the set (Tarantola, 1987). If the object function is convex in the entire parameter space, there is only one maximum and the solution is called unique. Geologically, stability and uniqueness are far more important than determining the precise parameters of the optimal stress. The data is called heterogeneous if different stresses have activated the different subsets of faults. The heterogeneity of fault-slip data may affect both the stability and uniqueness.

The stability, uniqueness, and precision of the solution depend on the topography of the object function over the parameter space, and the topography depends on given data set. Small variations of data may result in small variation of the function. If the function has only one narrow peak in the entire parameter space, the solution is unique and stable (Fig. 1a). In contrast, if the maximum point is on a plateau, a small change in the shape of the plateau shifts the maximum point far away (Fig. 1b). This is a case of an unstable solution. If the function has multiple peaks with similar height (Fig. 1c), the optimal solution that is given by the highest one may be unstable and the physical meaning of the solution is vague. Does the correct solution coincide with one of the peaks? Or does the object function always have only one, narrow peak? The purpose of this paper is, in the first place, to answer these questions by visualizing the topography in four-dimensional parameter space.

Natural data are often heterogeneous. For this reason, before making use of the conventional inverse method, we have to classify the subsets at outcrops to make the subsets homogeneous. The separation of stresses from those data is a major problem. The classification is possible, but usually difficult and sometimes subjective, so that the problem is serious. Old terrains have experienced long and complex tectonic histories, allowing us to acknowledge several field criteria for the classification (Lisle and Vandycke, 1996). However, few criteria are found from young faults in active terrains such as the faults in mid Quaternary forearc basin sediments near the triple plate junction off central Japan (Yamaji, 2000a). Numerical or automatic classifiers are needed. To meet this demand, such methods are proposed by several researchers (Angelier and Manoussis, 1980; Nemcok and Lisle, 1995; Yamaji, 2000b).

The second purpose of this paper, to show the visualization technique that will be presented in the following sections, is useful to separate stresses from heterogeneous fault-slip data. In addition, the resolution of this graphical technique is compared with that of Yamaji's (2000b) multi-inverse method. And, finally, the technique is shown to be an extension of the right dihedral method (Angelier and Mechler, 1977) which is able to indicate not only possible stress orientations but also possible stress ratios.

The present technique depends on Angelier's (1979, 1984) inverse method, which therefore is outlined in the following section.

2. Methodology

2.1. Conventional inverse method

Stresses are determined from fault-slip data that consist of the orientation of fault planes, the direction of slickenside striations, and the sense of movement. Given a stress tensor, the Wallace–Bott hypothesis allows the prediction of the slip direction of the faults. Let d_i be the angular misfit between the predicted and observed slip directions of the ith fault. Note that $0 \leq d_i \leq 180°$. The optimal stress tensor is determined by maximizing the fit of the assumed stress to the data:

$$F = \sum_{i=1}^{N} w(d_i) \tag{1}$$

where N is the number of faults, and

$$w(d) = 1 - \sin^2 d/2 \tag{2}$$

is the function for the evaluation of fit used by Angelier (1990). The shape of the function is arbitrary: the only requirement is that it is not a decreasing function of d. If

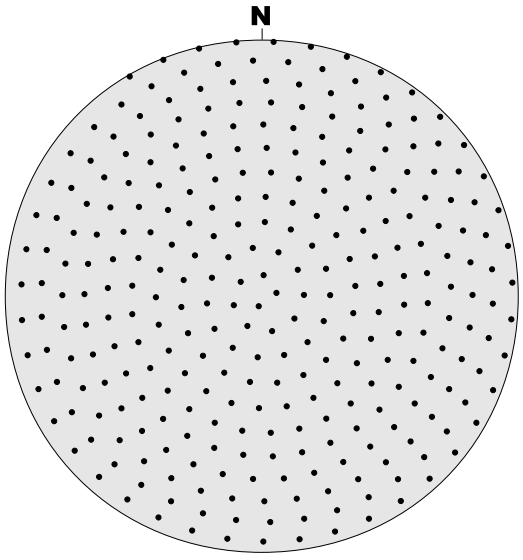

Fig. 2. Lower-hemisphere, equal-area projection of 300 directions of σ_3-axis used as computational grid points. About the directions, σ_1-axis is rotated with an interval of 18°.

the data set is heterogeneous, the influence of outliers should be suppressed to make the inversion robust and to detect the most significant stress. To this end, Angelier (1979) recommends the function of the form:

$$w(d) = \begin{cases} 1 - \tan d & (0 \le d \le 45^\circ) \\ 0 & (45^\circ < d). \end{cases} \quad (3)$$

The slip direction predicted by the Wallace–Bott hypothesis does not depend on all stress components, but on the direction of principal stress axes and the shape of Lamé's stress ellipsoid (McKenzie, 1969). The shape is represented by Bishop's (1966) stress ratio:

$$\Phi_B = \frac{\sigma_2 - \sigma_3}{\sigma_1 - \sigma_3}, \quad (4)$$

where σ_1, σ_2 and σ_3 are the principal stresses. As $\sigma_1 \ge \sigma_2 \ge \sigma_3$, it is seen that $0 \le \Phi_B \le 1$. We use the sign convention that compression is a positive stress. Axial compression ($\sigma_3 = \sigma_2 < \sigma_1$) and axial tension ($\sigma_3 < \sigma_2 = \sigma_1$) are represented by $\Phi_B = 0$ and 1, respectively. Triaxial stresses are indicated by intermediate ratios. The direction of the principal axes is described by Euler angles θ, ϕ, and ψ (Goldstein, 1980). Accordingly, the inversion determines the four parameters θ, ϕ, ψ, and Φ_B of the optimal stress by the scheme to seek the maximum point of the function $F(\theta, \phi, \psi, \Phi_B)$ in the four-dimensional parameter space, where F is the object function defined by Eq. (1). In the following sections, the principal directions are used instead of the Euler angles, because of the difficulty of understanding the principal directions from the angles.

Table 1
The object function, F, for data set A (Fig. 3) evaluated at the computational grid points listed in the ascending order of F. σ_1- and σ_3-directions are indicated by their azimuth (a) and plunge (p) angles

Relative fit	Computational grid point				
$F - F_{min}$	σ_1-axis		σ_3-axis		Φ_B
	a	p	a	p	
0.000	194	63	63	19	0.6
0.000	194	63	63	19	0.7
0.065	182	55	63	19	0.7
0.140	174	47	63	19	0.7
0.225	182	55	63	19	0.6
0.260	187	51	59	27	0.6
⋮	⋮	⋮	⋮	⋮	⋮
39.095	85	3	184	71	0.2
39.380	271	0	1	17	0.0
39.390	268	0	358	9	0.0
39.430	88	0	178	13	0.0
39.765	264	1	4	83	0.1
39.860	85	3	184	71	0.1
39.900	270	0	0	34	0.0
39.975	89	0	179	21	0.0
40.130	90	0	180	5	0.0
40.910	264	2	164	79	0.1

2.2. Visualization of the topography of F

Computer programs (main and post processors) were developed to visualize the topography of the object function, F, over the parameter space. The main processor calculates the fit at all grid points of computational mesh in the parameter space. The post processor projects the topography onto a plane to visualize the topography.

The mesh was generated as follows. Rakhamanov et al.'s (1994) algorithm was used to generate 300 directions for σ_3 axis with nearly equal intervals (Fig. 2), and the direction of σ_1 axis is rotated about the σ_3 axis with an interval of 180°/$18 = 10°$. The stress ratio, Φ_B, is divided into 11 grades from 0 to 1 with an interval of 0.1. The total number of grid points is $300 \times 18 \times 11 = 59{,}400$. The angular distance of neighboring σ_3 directions shown in Fig. 2 is not exactly constant, and its mean is $8.3 \pm 1°$ (one standard deviation).

The main processor calculates the fit, F, at all grid points and tabulates the results with the direction of stress axes and stress ratio arranged in the ascending order of F. An example is shown in Table 1. The post processor represents the table using a couple of color stereograms: both are lower-hemisphere equal-area plots, and the left and right stereograms always indicate the direction of σ_1 and σ_3-axes, respectively. Φ_B and F are indicated by hue and saturation of color, respectively. Color saturation is a degree to which a pure color of the spectrum is diluted by white. Only the relative value of F is meaningful, so that the relative fit, defined as F minus the minimum F, is represented by color saturation. High and low relative fits are indicated by pure and whitish colors, respectively.

The parameter space is four-dimensional, so that stereographic projection involves the reduction of information. Specifically, many points with the same σ_3 direction but

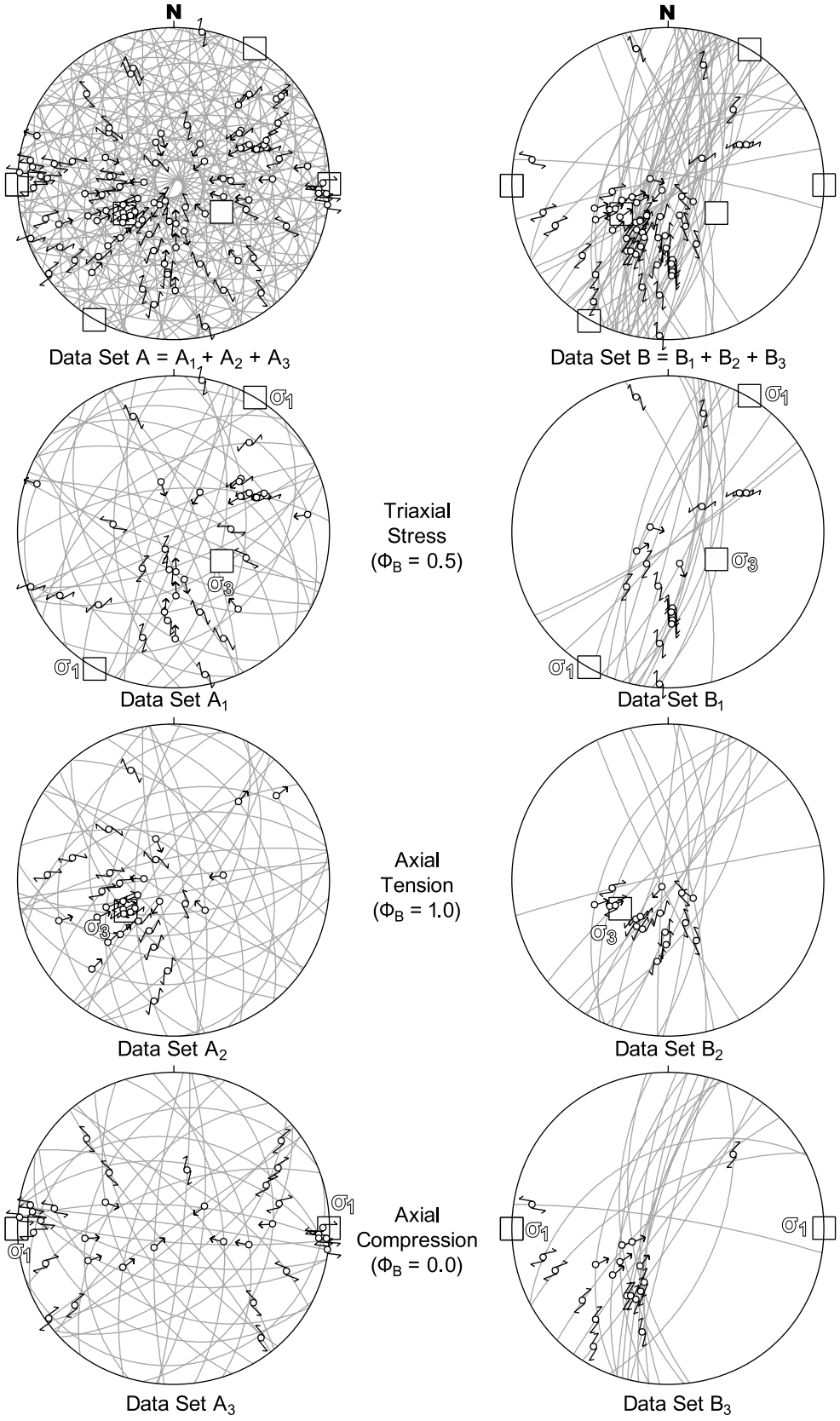

Fig. 3. Numerically generated fault-slip data. Lower-hemisphere, equal-angle projection. The direction of assumed stress axes is indicated by squares. The fault-slip data A_1, A_2, and A_3 are homogeneous: the members of each set are assumed to be activated by a state of stress. The sets are combined to make a heterogeneous data set A. The heterogeneous data set B is composed as A, but has less faults, and smaller variation of fault orientations. The orientations are the same with data set O (Fig. 4). The members of the subsets B_1, B_2, and B_3 are assumed to be activated by the same stress as A_1, A_2, and A_3, respectively.

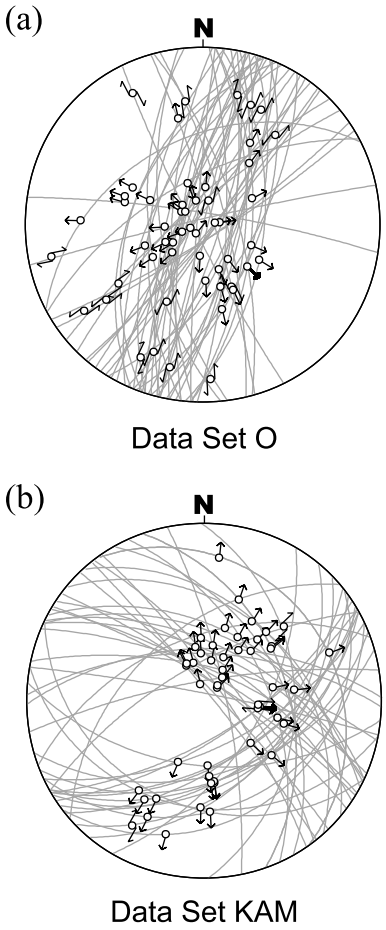

Fig. 4. Natural, heterogeneous, fault-slip data set O and KAM. The former set was obtained in the Otadai Formation, central Japan, by Mino and Yamaji (1999). The number of data is 53. The data set KAM is listed by Angelier (1990), and was collected from the Kamogawa area near the location of data set O. The number of data is 50.

different σ_1 directions are projected on the same point among those shown in Fig. 2. To minimize the overlapping projection, the plotted points were dispersed around the points within a radius of 8°. Consequently, the stereograms are filled with dots with various colors, although the fit is calculated at discrete grid points. The color plotting is executed in the ascending order of F, so that the color dots with lower F are hidden by those with higher F.

2.3. Multi-inverse method

The multi-inverse method (Yamaji, 2000b) is a numerical technique to separate stresses from heterogeneous fault-slip data, and is based on the conventional inverse method and on resampling statistical technique as the Jackknife and Bootstrap methods (Quenouille, 1949; Efron, 1979). They solve statistical problems by resampling data, and determine optimal parameters for each subset of data. The core of the multi-inverse method is as follows. Suppose we have N fault-slip data, and make k-element subsets. Consequently, we have a number of

$$ {}_N C_k = N!/k!(N-k)! \tag{5} $$

subsets, where ${}_N C_k$ is a binomial coefficient. The second step is that the optimal stress is determined by the classic inverse method for each subset—we have ${}_N C_k$ stresses that are represented by points in the four-dimensional parameter space. Then, statistically significant stresses make clusters in the space. The clusters are visualized by stereograms. Note that the choice of combination number, k, in Eq. (5) is arbitrary. Accordingly, we can confirm the significance of the clusters by the convergence of clustering with the increase of the number.

3. Test data

To test the topography of the object function through this graphical representation, artificial and natural data sets A, B, O were prepared. All of them are characterized by multiple solutions and therefore are heterogeneous. The natural data set KAM of Angelier (1990) is also used. The artificial data were generated as follows. First, 100 fault planes were generated with their poles being oriented with uniform angular intervals by Rakhamanov et al.'s (1994) algorithm. The faults were then divided into three subsets A_1, A_2, and A_3 to which different stresses are applied. They are a triaxial stress ($\Phi_B = 0.5$), axial tension and axial compression, respectively, with different principal directions. The slip directions were calculated on the basis of the Wallace–Bott hypothesis. The direction of stress axes and stress ratio of the stresses are shown in Fig. 3 with the generated fault-slip data. Each of the resulting data sets A_1, A_2, and A_3 is homogeneous, and the heterogeneous data set A was created by the concatenation of the three subsets.

As for the natural data set O, we use 53 faults observed in the mid Quaternary fore-arc sediment, called the Otadai Formation, in central Japan (Fig. 4a). They were collected by Mino and Yamaji (1999) and Yamaji (2000a) applied the multi-inverse method to them and detected three stresses.

One more set of artificial and heterogeneous data was created and will be labeled as B by use of the fault planes of set O in the following discussions. The orientation of faults is the same as set O. The members of set O were divided into three subsets B_1, B_2, and B_3 to which were applied the same stresses that were used for the subsets A_1, A_2, and A_3, respectively. The heterogeneous data set B is the concatenation of the subsets B_1, B_2, and B_3 (Fig. 3). The stresses that should be detected are the same for sets A and B. However, the number of faults in B is about the half of those in A. In addition, the variation of fault orientations is smaller in B than A. Therefore, detecting the solutions from set B is more difficult than from set A.

The natural data set KAM (Fig. 4b) consists of 50 faults

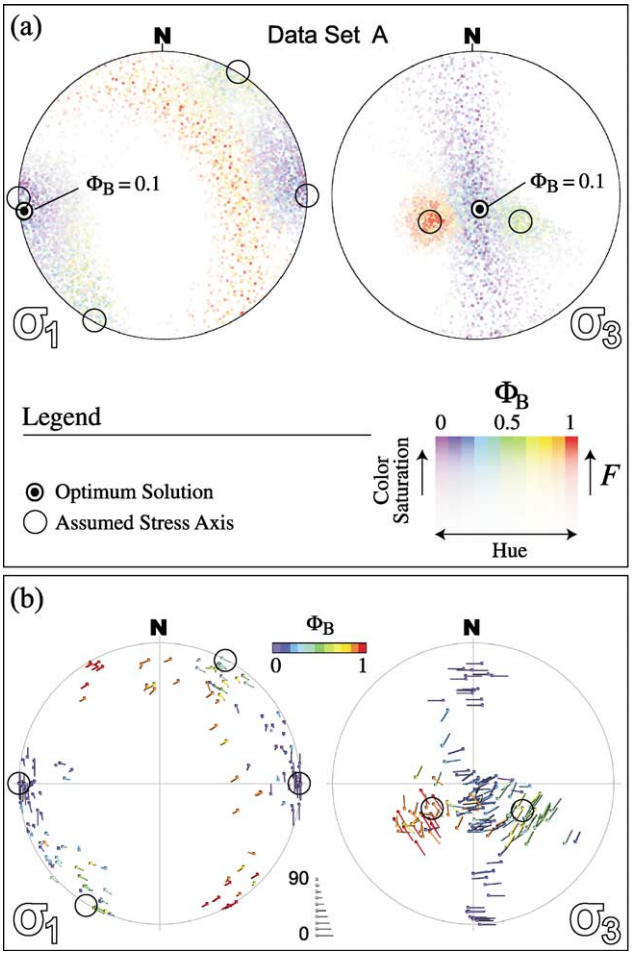

Fig. 5. (a) Graphical representation of the object function F for the artificial and heterogeneous data set A. The direction of stress axes is plotted on Schmidt nets with color-coded fitness, F, and stress ratio, Φ_B. Lower-hemisphere projection of σ_1 (left) and σ_3 (right) directions. Open circle, the directions of assumed stress axes in Fig. 3. The color spots and girdles represent peaks and ridges of the function in the parameter space. Reddish spot on the right stereogram shows the peak at the stress state whose σ_3-direction is indicated by the spot and the color indicates the state of stress being axial tension. As it is symmetric about the axis, the corresponding σ_1-directions are indicated by reddish great-circle girdles in the left stereogram. The violet spot in the left one shows that axial compression with E–W horizontal σ_3 axis is another significant peak. Greenish spots in both stereograms represent the third peak: triaxial extension with intermediate stress ratio and NNE–SSW σ_1, and highly plunging σ_3 axis to SE direction. The color spots appear at or near the assumed stress axes with correct stress ratios. The optimal solution determined by conventional inverse method with the function Eq. (3) is also plotted. (b) The result of multi-inverse method applied to data set A. Open circles indicate the direction of assumed stress axes. Clusters of dot–bar symbols with the same color and same bar direction represent significant stresses. Each symbol represents a state of stress: stress ratio is represented by color, and the direction of stress axes is indicated by the position and direction of the symbol. The directions of σ_1 and σ_3 axes are indicated by dots on lower-hemisphere equal-area projections on the left and right, respectively. In the left figure, the direction of bars extending from the dots indicates the azimuth of the corresponding σ_3-direction. The length of bar designates the plunge of the direction. On the right equal-area net, the role of the bar and dot are assigned inversely. The length and direction of the bar indicate the σ_1-direction. MIM was applied with the combination number and enhancing parameter at 4 and 7, respectively. See Yamaji (2000b) for the details of the parameters.

with normal or oblique-normal sense of shear, and is taken from Angelier (1990). He also shows the optimal stress for the data set. Both the areas where the data sets O and KAM were collected are in central Japan, and are about 40 km apart. The data set KAM was obtained from ophiolitic rocks, which are assigned to the Paleogene (Suzuki et al., 1984; Mohiuddin and Ogawa, 1996). However, field observations allowed Angelier to select faults of a young extensional event out of a lot of older faults.

The object function, F, is evaluated for data sets A, B, and O with Eq. (3), but that for KAM is done with Eq. (2).

4. Results

4.1. Data set A

The fit, F, at the computational grid points is listed in Table 1 for this data set in the ascending order of F, though only the top and bottom of the list are shown. The graphic representation was constructed and is shown by the pair of stereograms in Fig. 5a. This figure clearly shows that the function has multiple peaks in the four-dimensional parameter space. Color spots and girdles represent the peaks. They look nebulous because the points were plotted with the dispersion that is explained in Section 2.2. Open circles in this figure indicate the assumed axial directions shown in Fig. 3. There is a N–S trending girdle of violet dots in the right stereogram. The hue indicates a low value of Φ_B and thus $\sigma_2 \cong \sigma_3$. The state of stress is nearly axial, so that violet spots appear in the left stereogram normal to the girdle. The reddish girdle in the left stereogram corresponds to the spot with the same color in the right stereogram, indicating that an axial tension is also a state of stress with high F. Greenish spots appear in both stereograms, indicating that there is an additional peak in the parameter space corresponding to a state of stress with an intermediate Φ_B. Fig. 5a shows that the direction and stress ratio of the spots coincides with those of the assumed stresses that are designated by circles in the figure. Consequently, this graphical representation not only shows the topography, but also allows us to separate stresses from the formidably heterogeneous fault-slip data.

Among the spots, the reddish one is the most compact, and thus the most precisely and stably determined stress on this graphic representation. Principal axes are precisely determined if slip vectors are nearly parallel to the axes (Gephart and Forsyth, 1984). This condition holds the most in subset A_2 (Fig. 3) whose members were activated by the axial stress represented by the reddish spot, resulting in the compact spot. Violet spots are vague and their centers are rotated about the vertical by $\sim 10^\circ$ away from the assumed stress axis, although the spot encompasses the optimal stress axes. Greenish spots are vague and elongated, and mixed with the violet ones at their borders. Therefore, the triaxial stress represented by the greenish spots is the

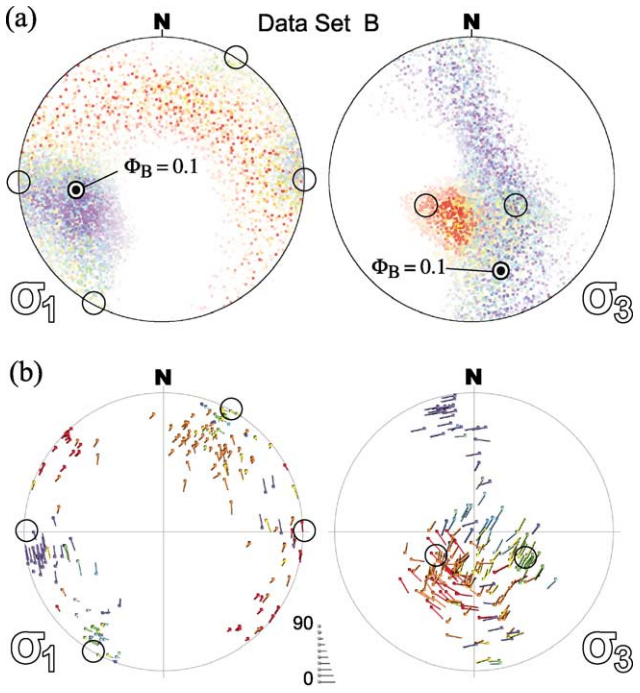

Fig. 6. (a) Graphic representation of the object function for data set B. Note that the optimal solution with stress ratio at 0.1 has stress axes that coincide with none of the assumed stress axes. (b) The result of the multi-inverse method that was applied to the same data. See Fig. 5 for legend.

most difficult stress to detect by the conventional inverse method.

The last line of Table 1 represents the optimal stress. This solution has an error that is derived from the discrete computational grid points. The representative angular interval of between the points is 10° or less. The solution is plotted in Fig. 5a, also. The optimal σ_1-direction agrees with the assumed direction of the axial compression within the error. The optimal solution has $\Phi_B = 0.1$, but the assumed value was $\Phi_B = 0$. The heterogeneity of the data has shifted the optimal solution from the assumed parameters of the axial compression. The color spots and girdle patterns clearly indicate that the given fault-slip data are heterogeneous, and the optimal solution alone does not explain the whole fault activity. However, considering the heterogeneity of data set A, the inversion is successful in determining one of the assumed stresses. In this calculation, F was evaluated with Eq. (3), which was presented for fault analysis by Angelier (1979) to process heterogeneous data. However, the solution is somewhat unstable, because the color saturation of the violet spot is not so different from that of the reddish spot. This means that the peaks represented by the spots have similar values of F.

Fig. 5b shows the result of the multi-inverse method applied to data set A. Clusters of dot–bar symbols with the same color and the same bar direction indicate significant stresses determined from the data set. Insignificant solutions were cut-off by the following procedure (Yamaji, 2000b). The method was applied with the combination number, k, in Eq. (5) being equal to four, therefore we have ${}_{100}C_4 = 3{,}921{,}225$ optimal stresses. They are too many to plot on a stereonet. Let m be the number of solutions at a computational grid point that represents a state of stress. The number m is an attribute of a grid point. Then, we calculate the standard deviation, s, of the numbers. The parameter s is used to thin out the solutions and to enhance significant stresses by plotting only m/es dot–bar symbols on stereograms, where the natural number e is called enhancing parameter. If $m/es < 1$, no symbol is plotted. We used a value of $e = 7$ for Fig. 5b.

The assumed stresses are successfully detected by this method, also. Among the clusters, the most divergent is the one indicating axial tension, contrary to the graphical representation (Fig. 5a). The clusters of greenish and bluish symbols in the left stereogram are contiguous in the SW quadrant, similar to the situation in Fig. 5a that the violet to blue spot is mixed with the greenish spot at their border.

4.2. Data set B

This data set is more difficult than set A for stress inversion, because of the smaller variation of fault orientations, and the smaller number of faults. The topography of the function, F, is shown in Fig. 6a. Color spots and girdle patterns in this figure show clearly that the function is multi-modal. The violet spot in the left stereogram should be centered at horizontal and due west direction, but is shifted by ~40°. The greenish spot that indicates the assumed triaxial stress is also shifted and spread so as to be mixed with the violet spot in the left stereogram of Fig. 6a. The greenish spot is also spread in the right stereogram and mixed with the violet girdle. The reddish spot in the right stereogram is also spread in comparison with Fig. 5a, and is rotated counterclockwise by ~30° about the vertical. However, the spreading of the red spot is smaller than the violet and green spots in the left and right stereograms, respectively. The reddish spot is the more compact and has a higher saturation than the violet and greenish spots, as for the case of data set A.

For data set B, the conventional method determines the optimal stress that has the stress ratio at 0.1, indicating that it is nearly an axial compression. The axis lies in the violet spot. The optimal σ_1-direction is different from that of the assumed axial compression by ~30°. The similar color saturation of the reddish and violet spots suggests the optimal solution is unstable.

The same data set is processed by the multi-inverse method, and the results are shown in Fig. 6b. The clusters of violet, greenish, and reddish dot–bar symbols appeared near the direction of assumed stress axes, indicating the method successfully separated the stresses. However, the clusters are more divergent than those of Fig. 5b. The reddish one is most scattered. Consequently, this method seems more robust in processing this data set than the present graphical representation to separate stresses.

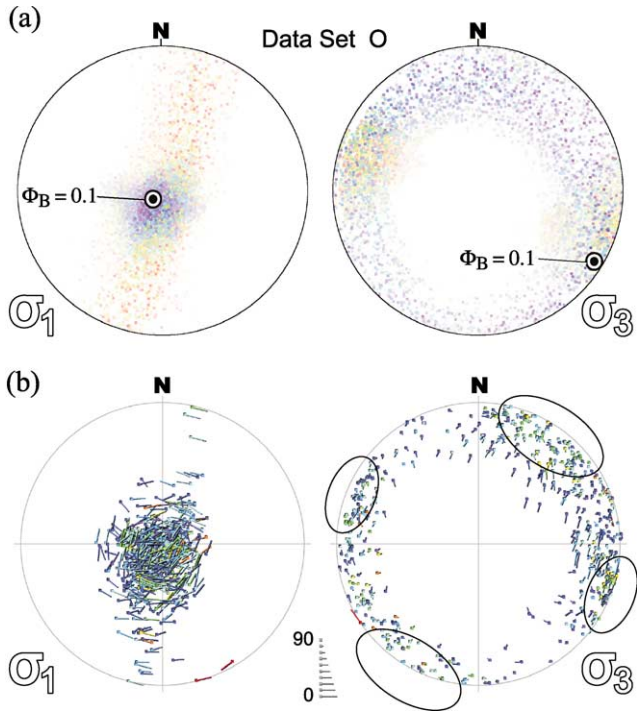

Fig. 7. (a) Graphic representation of the object function for the natural data O. Optimal stress was determined as nearly axial, vertical compression with $\Phi_B = 0.1$ and NE-trending σ_3 axis. (b) The result of multi-inverse method that was applied to the same data. See Fig. 5 for legend. Clusters of green symbols are encircled in the four quadrants in the right figure.

4.3. Data set O

These are natural data collected from Quaternary sediments in central Japan by Mino and Yamaji (1999). Because the data are natural, no one knows the true stress(es) recorded in the data. The graphical representation of the function, F, is shown in Fig. 7a. There are color spots and girdles, indicating that the function is multi-modal. In the left stereogram, violet and greenish spots appear commonly at the center. A reddish girdle pattern is parallel to the common direction, and the girdle pole is oriented in ESE–WNW direction. This direction is indicated by reddish spots in the right stereogram of Fig. 6a. Greenish spots overlap the reddish ones. In addition, the directions represented by the reddish and greenish spots are parallel to the plane indicated by the violet girdle pattern in the right stereogram. These observations indicate that the three states of stresses represented by the color spots and girdles have common directions of stress axes, but are different only in their stress ratios. They are determined by NNE–SSW trending dip-slip normal faults among the given data. The slip directions of the faults caused by the three stresses are indistinguishable because the trend of the dip-slip faults is approximately perpendicular to the σ_3-direction, so that the stresses are equally possible solutions. Yamaji (2000b) calls stresses of this relationship ‘associated stresses’.

The optimal stress determined by the conventional method is also shown in Fig 6a. The state of stress is near vertical axial compression. The optimal σ_1 axis lies in the direction shown by the violet spot. The overlapping color spots and girdles indicate that this solution is not unique. However, color saturation of the violet spot is greater than for the greenish and reddish ones, suggesting that the solution is stable. However, the violet to blue girdle pattern in the right stereogram of Fig. 6a suggests that the optimal σ_3-direction is much less definite and less stable than the σ_1-direction.

Although the optimal solution is stable, there are many outliers that are not compatible with the solution. The vertical, nearly axial compression is the optimal stress, which activates any fault as a normal fault. However, there are strike-slip and oblique-slip faults with sinistral and dextral senses of shear. This means that such vertical compression as the optimal solution is not enough to account for the whole fault activity. The conventional method and the present graphical representation fail to separate stress(es) not in the association relationship.

The stability of the solution is supported by Mino and Yamaji’s (1999) study. Following Angelier and Manoussis (1980) and Angelier (1994), Mino and Yamaji divided this data set into two subsets by the fact that the misfits, d_i, for the optimal stress have bimodal distribution. Accordingly, they selected the members with smaller misfit and calculated the optimal solution for them. The solutions obtained by the first and second inversions were identical, through the first one was applied to the heterogeneous data. This demonstrates the stability of the solution. The solution for the remaining set of data was a strike-slip regime of stress whose σ_3-axis lay in NE–SW trend with $\Phi_B = 0.58$.

Fig. 6b shows the solution of multi-inverse method applied to the same data set. The vertical axial compressive and associated ESE–WNW triaxial, horizontal extensional stresses are detected. The former is indicated by the cluster of bluish dot–bar symbols at the center of the left stereogram. The latter is represented by the cluster of green symbols encircled in the NW and SE quadrants of the right stereogram. In addition to these states of stress, a NE–SW-trending extensional stress is detected. The solution is represented by the cluster of green symbols encircled in the NE and SW quadrants of the right stereogram. The strike-slip and oblique-slip faults that are not compatible with the associated stresses are explained by the NE–SW extensional stress.

4.4. Data set KAM

The graphical representation of the function, F, for this data set is shown in Fig. 8a. Angelier (1990) determined the optimal stress with the function identical with Eq. (2), therefore, the graphical representation was composed with the same function. In the left stereogram, dots with cold colors make clusters at the center, indicating that the state of stress with a vertical σ_1 axis and low stress ratio is the most

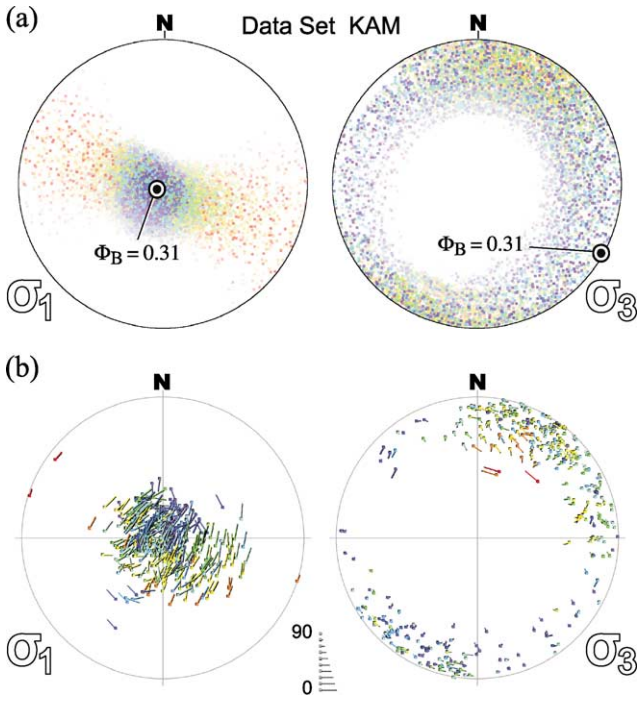

Fig. 8. (a) Graphic representation of the object function for the natural data KAM. The function was evaluated in this case with the function Eq. (2). The optimal solution with $\Phi_B = 0.31$ is also shown. (b) The result of multi-inverse method that was applied to the same data. See Fig. 5 for legend.

probable solution. Green, yellow, and red dots are sparse and have low saturation, so that the stresses represented by those colors are less likely. In the right stereogram, violet to light blue dots make a nearly horizontal, broad girdle pattern. In addition, green to red dots make clusters at horizontal, NNE and SSW directions. The spots overlap with the girdle pattern, so the quadrants are plotted with mixed colors.

Angelier (1990) determines the optimal stress that is shown in Fig. 8a. The optimal stress ratio is 0.31, which should be represented by light blue spots in the figure. However, no such spot appeared in either stereograms. Only a spot with mixed cold colors appeared at the optimal σ_3-direction. Therefore, the peak represented by the optimal solution is one of many peaks with different stresses: the solution is not unique and therefore unstable. The instability is indicated by the fact that the central spot of the left stereogram consists of an equal amount of violet and light blue dots. In addition, there are many NW–SE-trending, dip-slip normal faults in the data (Fig. 4b) that are not explained by the optimal stress alone. The data are heterogeneous. NNE–SSW-trending, horizontal, extensional stress, which is represented by the mixed color spots in the right stereogram. is a possible solution, though the possibility is less than the vertical nearly axial compression that is represented by the central spot of the cold color. The extensional stress helps explain them.

The result of the multi-inverse method applied to the data set is shown in Fig. 8b. We recognize two stresses there: vertical axial compression with low Φ_B and NE–SW-trending horizontal extension with $\Phi_B = 0.5$. The latter may be divided into two clusters in NNE–SSW and E–W trends, or a poorly resolved extensional stress in the NE quadrant. Most of the members of this data set are nearly dip-slip normal faults that have slip vectors trending in N–S to NE–SW and E–W directions (Fig. 4b). The divergent trend of the normal faults results in the horizontal green cluster elongated from north to east in the right stereogram of Fig. 8b.

In the SE quadrant of the right stereogram of Fig. 8b, there are light blue dot–bar symbols of which stress ratio and stress axes are, indeed, consistent with the optimal solution. However, symbols with that color do not make clusters, indicating that the optimal solution is much less significant than the stresses that are the vertical axial compression and NE–SW extensional stress.

Data set KAM was collected from the Kamogawa area, 40 km away from the area where data set O was obtained. The above two stresses are detected from both data sets. However, the most significant stress determined from data set O (NW–SE tension) is not obtained from set KAM.

5. Discussion

We have processed artificial and natural fault-slip data with heterogeneity. It has been shown that the conventional method can detect one of the correct stresses if the misfit is evaluated by functions like Eq. (3) that minimize the effect from outliers, and if the fault orientations have a large variation. One of the assumed stresses was detected with an error of no less than 30° for data set B that has a smaller number of faults with less variation in fault orientations than set A. The method can, at best, determine one of the correct stresses using evaluation functions like Eq. (3).

The reliability of the optimal stress is not obvious in the conventional method. Angelier (1990) estimates the reliability by a parameter called RUP, which is a measure of the mean misfit of the predicted and observed slip directions. However, the graphical representations in the last section clearly show that only one parameter, not only RUP but also any kind of parameter, is not enough at all to describe the reliability of the optimal solution. The parameter cannot characterize the complex topography of the function F. Graphical representation is the most suitable method to recognize such complex objects as Fry (1999) emphasizes.

The estimation of (paleo) stresses by the conventional method has been done in many areas over the world, although the heterogeneity of fault-slip data was not always critically investigated. Those studies without the check should be reevaluated.

It should be noted that the graphical representation is an extension of the right dihedra method, which was put forward by Angelier and Mechler (1977), but shows not only the possible principal directions but also possible stress

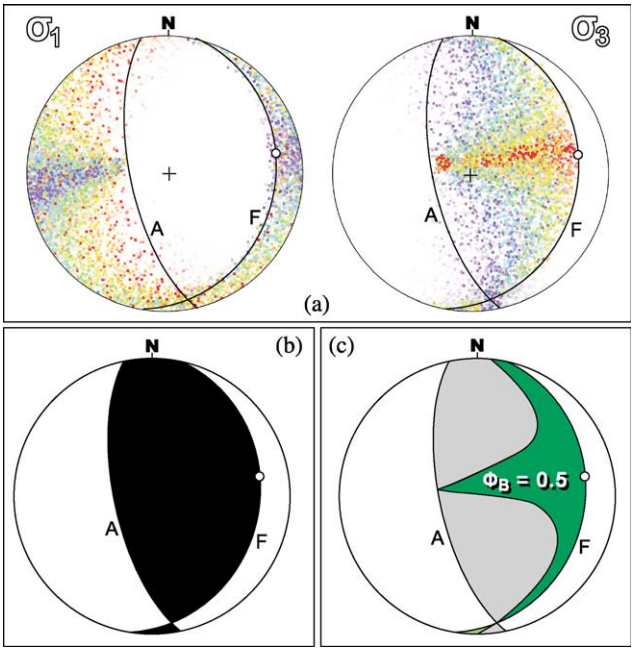

Fig. 9. (a) Graphic representation of the object function for a single thrust fault. Lower-hemisphere, equal area projection. Great circles labeled as A and F are the auxiliary and fault planes, respectively. The pole to the auxiliary plane is oriented parallel to the slip direction shown by open circles. (b) Possible σ_3 directions (black quadrants) determined by the right dihedra method for the thrust fault. (c) The increase of Φ_B reduces the possible σ_3 directions. Green regions show possible σ_3 directions for stresses with $\Phi_B = 0.5$. If $\Phi_B = 0$, both the green and gray regions are possible.

ratios. This is indicated by Fig. 9a that shows the F for a single thrust fault. The possible principal directions for the fault are indicated by quadrants defined by the fault and auxiliary planes by the right dihedra method, and the quadrants are shown by black and white quadrants on a stereogram (Fig. 9b). In addition, the present method shows the possible stress ratios. McKenzie (1969) obtained the analytic solution for possible combinations of principal directions and stress ratios for a single fault. Fig. 9c shows McKenzie's solution for the case of our thrust fault. Possible principal directions for a given stress ratio is shown on a stereogram

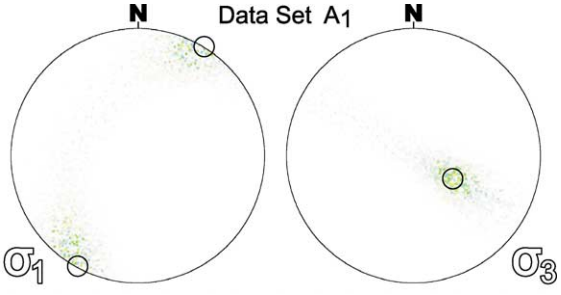

Fig. 10. Graphic representation of the object function for the homogeneous data set A_1 whose fault orientations and slip directions are shown in Fig. 3. Open circles indicate the direction of assumed stress axes. See Fig. 5 for legend.

by a pattern like a stingray or a ginkgo leaf (McKenzie, 1969; Fig. 3). Such patterns are found in Fig. 9a. For many faults, the function F of each fault is simply superposed by Eq. (1). Consequently, the graphical representation of F is an extension of right dihedra method so as to show possible stress ratios. The distribution of color dots in Fig. 9a is not bounded by the auxiliary plane, because the fit, F, for principal axes in the white quadrants in Fig. 9b is not always zero but varies in the quadrants. The right dihedra method is argued to be weak for heterogeneous data (Carey-Gailhardis and Vergely, 1992; Lisle and Vandycke, 1996). However, this extension of the method can separate stresses from those data if fault orientations have a large variation and if homogeneous subsets have a similar number of faults as for the case of set A.

If conjugate faults were activated, plotting P and T axes on a stereogram for fault-slip data can separate principal axes (Twiss and Unruh, 1998). However, it is not always obvious whether observed heterogeneous faults are activated as conjugate faults in polyphase tectonics: conjugate faulting is not the only choice of fault activity when a three-dimensional strain is forced to the rock mass that encompasses the faults (Reches and Dieterich, 1983). The plotting of P and T axes detects principal stress axes from heterogeneous data, but the present graphic method shows not only principal axes, but also stress ratios.

It is interesting to apply the present graphical method to homogeneous data. Fig. 10 shows the uni-modal function, F, for the homogeneous data set A_1.

The members of the set were activated by the triaxial stress with NNE–SSW-trending horizontal σ_1 axis and with σ_3 axis steeply plunging in the SW direction (Fig. 3). The stress ratio was assumed to be 0.5, which is represented as green in the graphical representation. Fig. 10 shows that only greenish spots stand out at the expected principal directions, indicating that the function is uni-modal. If the given data are homogeneous, then the conventional method is able to detect the assumed stress. If they are heterogeneous, it can, at best, determine the most significant solution, but a conventional estimator such as RUP is not enough to understand the reliability of the solution. It is shown that the graphical representation of F makes heterogeneity obvious.

The present method visualizes $F$and Φ_B by color saturation and hue, respectively. The shortcoming of this method is that saturated yellow is less prominent than saturated violet, green, and red. There are certainly other methods of visualization. As an example, the function F is indicated by hue and the difference in stress ratio is shown by individual stereograms. Contours cannot show the variations of F over the stereograms, because many states of stress with one of the three stress axes in common share one point on a stereogram. The present method is better than this one in that the latter needs more space to draw stereograms. We have divided stress ratio into 11 grades between 0.0 and 1.0, so that 11 times more space is necessary. The present method plots color dots in the ascending order of F, and

the dots with smaller F are hidden by those with greater F. This procedure addresses the shortcoming.

The multi-inverse method outdid the present graphical method in the separation of stresses from heterogeneous data. The former can detect stresses whose axes are nearly parallel to most fault planes. However, the latter method becomes better than the former one if we process hundreds of fault data. The reason is that the time of computation does not inflate with the number of faults, N. The bottleneck of the method is in its graphic routine whose time of computation does not depend on N. It takes about 10 min to process a set of data by a personal computer with MMX Pentium processor, 166 MHz. In contrast, the multi-inverse method spends much more time that increases as N^k, where the integer k is typically between 4 and 7 (Yamaji, 2000b).

We have discussed the possibility of separating stresses from heterogeneous data sets. When we analyze natural data sets, errors are inevitable when measuring the orientation of fault planes and slickenside striations. Given slip vectors nearly parallel to principal stress axes, the inversion used in the conventional and multi-inverse methods is not tolerant of the error. Therefore, Gephart and Forsyth (1984) point out that the minimization of the angular misfit between observed and theoretical slip directions is vulnerable to the error. They recommend minimizing the variation in stress ratios that are compatible with observed data. However, stress ratios are sometimes difficult to determine, because stresses with similar principal directions but different stress ratios can result in the same fault activity (Yamaji, 2000b).

The main and post processors of the present graphical method are compatible with Windows Operating System, and are available from the Author's web page.

Acknowledgements

Many thanks to Y. Yamada for discussion. Helpful reviews by R.J. Lisle and R.J. Twiss improved the manuscript.

References

Amadei, B., Stephansson, O., 1997. Rock Stress and its Measurement. Chapman and Hall, London.

Angelier, J., 1979. Determination of the mean principal stresses for a given fault population. Tectonophysics 56, T17–T26.

Angelier, J., 1984. Tectonic analysis of fault slip data sets. Journal of Geophysical Research 89, 5835–5848.

Angelier, J., 1990. Inversion of field data in fault tectonics to obtain the regional stress—III. A new rapid direct inversion method by analytical means. Geophysical Journal International 103, 363–376.

Angelier, J., 1994. Fault slip analysis and paleostress reconstruction. In: Hancock, P.L. (Ed.). Continental Deformation. Pergamon Press, Oxford, pp. 53–101.

Angelier, J., Mechler, P., 1977. Sur une méthode graphique de recherche des contraintes principales également utiliable en tectonique et en séismologie: la méthode des dièdres driots. Bulletin de la Societé Géologique de France 7, 1309–1318.

Angelier, J., Manoussis, M., 1980. Classification automatique et distinction de phases superposées en tectonique cassante. Comptes Rendus Hebdomadaires des Seances de l'Academie des Sciences 290D, 651–654.

Bishop, A.W., 1966. The strength of solids as engineering materials. Geotechnique 16, 91–130.

Bott, M.H.P., 1959. The mechanics of oblique slip faulting. Geological Magazine 96, 109–117.

Carey, M.E., Brunier, M.B., 1974. Analyse theorique et numerique d'um modele mecanique elementaire applique a l'etude d'une population de failles. Comptes Rendus Hebdomadaires des Seances de l'Academie des Sciences 279D, 891–894.

Carey-Gailhardis, E., Vergely, P., 1992. Graphical analysis of fault kinematics and focal mechanisms of earthquakes in terms of stress; the right dihedra method, use and pitfalls. Annales Tectonicae 6, 3–9.

Dezayes, C.H., Villemin, T., Genter, A., Traineau, H., Angelier, J., 1995. Analysis of fractures in boreholes of the Hot Dry Rock project at Soultz-sous-Forêts (Rhine graben, France). Scientific Drilling 5, 32–42.

Dupin, J.M., Sassi, W., Angelier, J., 1993. Homogeneous stress hypothesis and actual fault slip: a distinct element analysis. Journal of Structural Geology 15, 1033–1043.

Efron, B., 1979. Bootstrap methods: another look at the jackknife. Annuals of Statistics 7, 1–26.

Fry, N., 1999. Striated faults: visual appreciation of their constraint on possible paleostress tensors. Journal of Structural Geology 21, 7–21.

Gephart, J.W., Forsyth, D.W., 1984. An improved method for determining the regional stress tensor using earthquake focal mechanism data: application to the San Fernando earthquake sequence. Journal of Geophysical Research 89, 9305–9320.

Goldstein, H., 1980. Classical Mechanics. 2nd ed. Addison-Wesley, Reading.

Lisle, R.J., Vandycke, S., 1996. Separation of multiple stress events by fault striation analysis: an example from Variscan and younger structures at Ogmore, South Wales. Journal of Geological Society of London 153, 945–953.

McKenzie, D., 1969. The relation between fault plane solutions for earthquakes and the direction of the principal stresses. Bulletin of Seismological Society of America 59, 591–601.

Mandl, G., 2000. Faulting in Brittle Rocks: An Introduction to the Mechanics of Tectonic Faults. Springer, Berlin.

Martin, P., Bergerat, F., 1996. Paleo-stresses inferred from macro- and microfractures in the Balazuc-1 horehole (GPF programme). Contribution to the tectonic evolution of the Cévennes border of the SE basin of France. Marine and Petroleum Geology 13, 671–684.

Mino, K., Yamaji, A., 1999. The separation of paleostresses from heterogeneous fault-slip data: the case of Boso area, Japan. Journal of Geological Society of Japan 105, 574–584.

Mohiuddin, M.M., Ogawa, Y., 1996. Middle Eocene to early Oligocene planktonic foraminifers from the micritic limestone beds of the Heguri area, Mineoka Belt, Boso Peninsula, Japan. Journal of Geological Society of Japan 103, 611–625.

Nelson, R.A., 1985. Geologic Analysis of Naturally Fractured Reservoirs. Gulf Publishing, Houston.

Nemcok, M., Lisle, R.J., 1995. A stress inversion procedure for polyphase fault/slip data sets. Journal of Structural Geology 17, 1445–1453.

Nieto-Samaniego, A.F., Alaniz-Alvarez, S.A., 1997. Origin and tectonic interpretation of multiple fault patterns. Tectonophysics 270, 197–206.

Pollard, D.D., 2000. Strain and stress: discussion. Journal of Structural Geology 22, 1359–1367.

Pollard, D.D., Saltzer, S.D., Rubin, A.M., 1993. Stress inversion methods: are they based on faulty assumptions? Journal of Structural Geology 15, 1045–1054.

Quenouille, M., 1949. Approximate tests of correlation in time series. Journal of Royal Statistical Society 11B, 18–44.

Rakhamanov, D.E.A., Saff, E.B., Zhou, Y.M., 1994. Minimal discrete energy on the sphere. Mathematical Research Letters 1, 647–662.

Reches, Z., Dieterich, J.H., 1983. Faulting of rocks in three-dimensional

strain fields I. Failure of rocks in polyaxial, servocontrolled experiments. Tectonophysics 95, 111–132.

Suzuki, Y., Kondo, K., Saito, T., 1984. Latest Eocene planktonic foraminifers from the Mineoka Group, Boso Peninsula. Journal of Geological Society of Japan 90, 479–499.

Tarantola, A., 1987. Inverse Problem Theory: Methods for Data Fitting and Model Parameter Estimation. Elsevier, Amsterdam.

Twiss, R.J., Unruh, J.R., 1998. Analysis of fault slip inversions: do they constrain stress or strain rate? Journal of Geophysical Research 103, 12205–12222.

Wallace, R.E., 1951. Geometry of shearing stress and relation to faulting. Journal of Geology 59, 118–130.

Yamaji, A., 2000a. Multiple inverse method applied to mesoscale faults in mid Quaternary sediments near the triple trench junction off central Japan. Journal of Structural Geology 22, 429–440.

Yamaji, A., 2000b. The multiple inverse method: a new technique to separate stresses from heterogeneous fault-slip data. Journal of Structural Geology 22, 441–452.